Effect of the temperature and magnetic field induced martensitic transformation in bulk $Fe_{45}Mn_{26}Ga_{29}$ alloy on its electronic structure and physical properties

Y. V. Kudryavtsev[a,1,], N. V. Uvarov[a], A. E. Perekos[a], J. Dubowik[b], L. E. Kozlova[c]

[a]*Institute of Metal Physics, NAS of Ukraine, Vernadsky 36,03142, Kiev, Ukraine*
[b]*Institute of Molecular Physics, PAS, M. Smoluchowskiego 17, 60-179 Poznań, Poland*
[c]*Institute of Magnetism, NAS of Ukraine, Vernadsky 36b, 03142, Kiev, Ukraine*

Abstract

Effect of the temperature and magnetic field induced martensitic transformation (MT) on the electronic structure and some physical properties of bulk $Fe_{45.2}Mn_{25.9}Ga_{28.9}$ Heusler alloy has been investigated. According to the experimental results of DSC, magnetic and transport measurements direct and reverse martensitic transformation without external magnetic field takes place within $194 \leq T \leq 328$ K temperature range with a hysteresis up to $\Delta T \approx 100$ K defined as $\Delta T = A_{f,s}$ - $M_{s,f}$, where $A_{f,s}$ and $M_{s,f}$ are the critical temperatures of direct and reverse martensitic transformation. External magnetic field of $\mu_0 H = 5$ T causes a high-temperature shift of MT temperatures. MT from parent austenite $L2_1$ phase to martensitic tetragonally distorted $L2_1$ one (i. e. to $L1_0$) causes significant changes in the electronic structure of alloy, a drastic increase in alloy magnetization, a decrease in the alloy resistivity, and a reversal of sign of the temperature coefficient of resistivity from negative to positive. At the same time experimentally determined optical properties of $Fe_{45.6}Mn_{25.9}Ga_{28.9}$ Heusler alloy in austenitic and martensitic states look visually rather similar being noticeable different in microscopic nature as can be concluded from first-principle calculations. Experimentally observed changes in the physical properties of the alloy are discussed in terms of the electronic structures of an austenite and martensite phases.

Keywords:
Heusler alloys, martensitic transformation, electronic structure, magnetic properties, optical properties
PACS: 64.70.Kb, 71.20.-b, 72.15.-v, 75.50.Bb, 78.20.-e

1. Introduction

Magnetic shape memory alloys (MSMAs) have found significant attention due to the possibility of rearrangement of martensite variants by external magnetic field. This property opens wide perspectives of their practical applications in medicine, robotics, active or passive damping [1]. Among MSMAs Ni-based Heusler alloys (HA) like Ni_2MnGa, Ni_2FeGa or Ni_2MnAl probably are most investigated [2, 3, 4]. In Ni-based MSMA HAs direct martensitic transformation (MT) from ferromagnetic (FM) austenite phase to FM martensite one is accompanied with a small reduction in alloy magnetization and an increase in alloy resistivity.

Quite distinct changes in these properties induced by a direct MT have been found in off-stoichiometric Fe_2MnGa alloys [5, 6, 7, 8]. The direct MT in these alloys is accompanied with a significant decrease in alloy resistivity and a transition from paramagnetic (PM) austenite to an FM martensite phase.

Phase equilibria upon phase transitions (like MT) are usually discussed in the framework of thermodynamics [9]. Effect of the electronic structures on such structural transformations was taken into account in a few reports [10, 11].

Among various experimental methods for studying of electronic structures of metals the optical spectroscopy (namely spectroscopic ellipsometry) is usually considered as such that manifests a higher compared to x-ray spectroscopy energy resolution (~ 0.01 eV) within $\pm$ 5 - 6 eV energy range near the Fermi level (E_F). Hence, spectroscopic ellipsometry was successfully employed for studying the solid-state reactions in multi-layered films [12], structural transformations in bulk metals and alloys [13]. For example, Sasovskaya *et al.* have shown experimentally that austenite to martensite transformation in NiTi alloy is accompanied with the appearance of a new intense absorption band in a near infrared region of spectra for martensite state [14]. It was also theoretically predicted that MT in Ni_2MnGa HA results from changes the electronic structure of alloy as well as its optical properties [15]. Furthermore, Gan'shina *et al.* have shown that the temperature induced martensitic transformation in $Fe_{48}Mn_{24}Ga_{28}$ alloy causes visible changes in the equatorial Kerr effect spectra which reflect the changes in the electronic structure and magnetic properties of alloy [16]. In this work, we try to consider the effect of the temperature and magnetic field induced MT in Fe_2MnGa alloy on its physical properties in close relation to the changes in the electronic structures of alloy studied theoretically and experimentally by employing the spectroscopic ellipsometry.

2. Experimental details

A slightly off-stoichiometric bulk polycrystalline Fe_2MnGa alloy was prepared by melting together pieces of Fe, Mn, and Ga of 99.99% purity in an arc furnace with a water-cooled Cu hearth under a 1.3 bar Ar atmo-

Email address: kudr@imp.kiev.ua (Y. V. Kudryavtsev)

[1]Corresponding author

2

sphere. The Ar gas in the furnace before melting was additionally purified by multiple remelting of a $Ti_{50}Zr_{50}$ alloy getter. To promote the volume homogeneity, the ingots were remelted five times. After ingot melting, the weight loss was about 3 %.

The actual composition of the fabricated bulk Fe_2MnGa HA sample was evaluated by using energy dispersive x-ray spectroscopy and found to be $Fe_{45.2}Mn_{25.9}Ga_{28.9}$.

The structural characterization of the sample was carried out at room temperature (RT) employing x-ray diffraction (XRD) in $\theta-2\theta$ geometry with Co-K_α (λ=0.17902 nm).

An SC 404 F1 Pegasus differential scanning calorimeter (DSC) was used to determine the phase transformation temperatures.

Magnetic properties of the bulk $Fe_{45.2}Mn_{25.9}Ga_{28.9}$ alloy were investigated over a temperature range $80 \leq T \leq 370$ K by measuring the DC-magnetic susceptibility in a weak magnetic field of 5 Oe and by measuring the magnetization over a temperature range $4 \leq T \leq 350$ K and a range of magnetic fields $0.5 \leq H \leq 50$ kOe by using the PPMS-P7000 system.

Transport properties were measured by using the four-probe technique over a range of temperatures $80 \leq T \leq 440$ K using the sample of $2.20 \times 1.25 \times 10.00$ mm^3 in size.

A bulk sample for optical measurements of about $10 \times 30 \times 2$ mm^3 in size was cut from the ingot employing spark erosion technique followed by mechanical polishing with diamond pasts. To eliminate surface contaminations induced by mechanical polishing, the sample before optical measurements was annealed at $T = 573$ K during 150 minutes at high vacuum conditions.

Optical properties [$Re(\sigma) = \omega\varepsilon_2/4\pi$ and ε_1, where σ is the optical conductivity (OC), ε_1 and ε_2 are the real and imaginary parts of the diagonal components of the dielectric function $\widetilde{\varepsilon} = \varepsilon_1 - i\varepsilon_2$] of the samples were measured by using a spectroscopic rotating-analyzer ellipsometer in a spectral range of 250 - 2500 nm (5.0 - 0.5 eV) at a fixed incidence angle of 73° at $T = 173$ and 373 K, respectively.

3. Results and discussion

3.1. Electronic structure

Figure 1 shows the spin-resolved energy dependencies of the density of electronic states [$N(E)$, DOS] for the stoichiometric Fe_2MnGa alloy with $L2_1$ and tetragonally distorted $L2_1$ (i. e. $L1_0$) types of structure calculated for lattice constants obtained from volume optimization procedure (for the $L2_1$ phase) and from experiment (for tetragonal phase). Calculations details can be found elsewhere [17]. It is seen that $N(E)$ dependence for $L2_1$ phase is characterized by energy gap near Fermi level (E_F) for minority bands and deep minimum for majority bands making this phase even not half-metallic but almost semi-metallic. At the same time for tetragonal phase narrow and intense maximum of the $N(E)$ dependence is observed at E_F for minority bands. It can be expected that such a drastic difference in DOS values at E_F for $L2_1$ and $L1_0$ phases will lead to some difference in transport properties of alloy and stability of these phases. Calculated magnetic moments for $L2_1$ and $L1_0$ phases of Fe_2MnGa
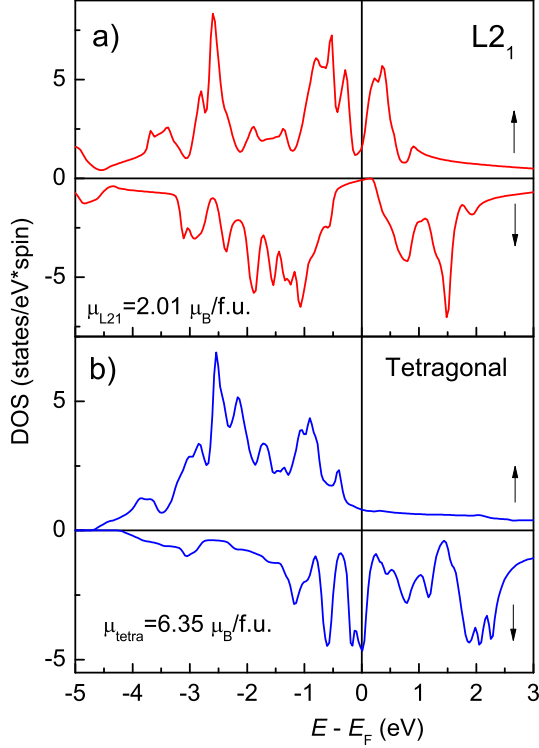
3

Figure 1: Spin-resolved density of states of stoichiometric Fe_2MnGa alloy calculated for a) $L2_1$ and b) tetragonal types of structure.
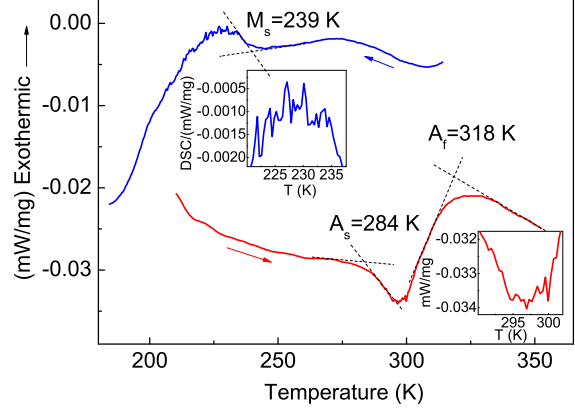

Figure 2: DSC patterns of bulk polycrystalline $Fe_{45.2}Mn_{25.9}Ga_{28.9}$ alloy during its cooling and heating. Insets show the enlarged view of the exothermic and endothermic parts of DSC plots.

alloy are $\mu = 2.01$ and 6.35 $\mu_B/f.u.$, respectively.

3.2. Crystalline structure

DSC measurements on sample heating and cooling clearly show an existence of exo- and endothermic processes displaced in the temperature and concerned probably with direct and reverse martensitic transformations in the alloy (see Fig. 2) [5, 6]. Unfortunately, M_f temperature using DSC plot is impossible to determine. Fine structures of DSC plots within temperature ranges of direct and reverse martensitic transformations indicate on the multiple-step-transformation process [i. e. a step-like process of increase (decrease) in a volume of martensitic phase] in alloy taking place at somewhat different temperatures due to probably compositional heterogeneousness. Obtained DSC data agree with the results of dilatometric measurements of bulk $Fe_{45.2}Mn_{25.9}Ga_{28.9}$ alloy upon its cooling and heating (see Fig. 3). These results show that direct martensitic transformation is started much below RT at $M_s \approx 240$ - 255 K, while the reverse martensitic transformation is finished above RT at $A_f \approx 318$ - 327 K. Thus, corresponding heat treatments will allow us to fix at RT either austenite or martensitic phases.

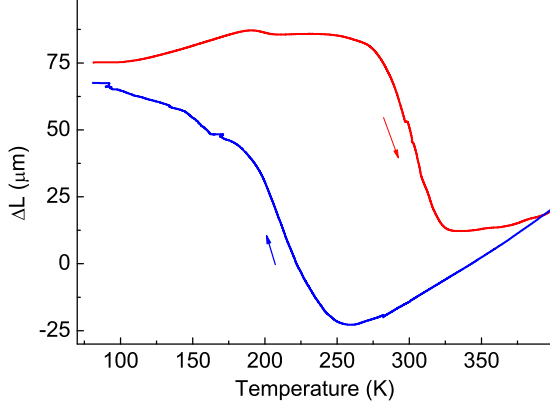Figure 4 presents RT experimental XRD patterns of preliminary heat treated

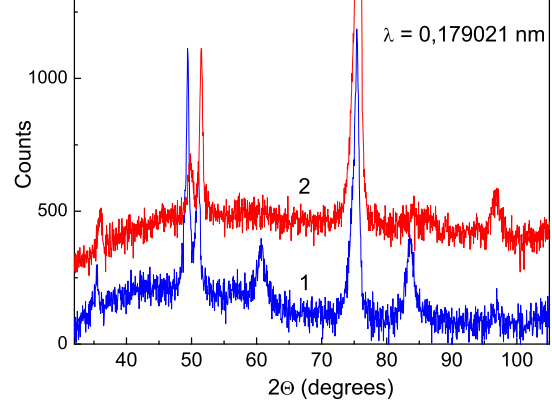Figure 3: Effect of the temperature on extension of bulk $Fe_{45.2}Mn_{25.9}Ga_{28.9}$ alloy upon its cooling and heating.

Figure 4: RT experimental XRD patterns for bulk $Fe_{45.2}Mn_{25.9}Ga_{28.9}$ alloy sample subjected to 1) its cooling down to $T = 78$ K and 2) heating up to $T = 373$ K.

$Fe_{45.2}Mn_{25.9}Ga_{28.9}$ alloy sample. The comparison of the obtained experimental XRD patterns with the results of XRD modelling (see Fig. 5) allows us to conclude that after heating up to $T=373$ K $Fe_{45.2}Mn_{25.9}Ga_{28.9}$ HA at RT contains mainly L2$_1$ phase with the lattice parameters of $a = b = c = 0.5829$ nm [superstructure lines (111), (200), (311), (331) and (420) are clearly seen] with the small admixture of, probably, tetragonal phase (reflection at $2\Theta = 49.77°$). After cooling down to $T = 78$ K at RT the $Fe_{45.2}Mn_{25.9}Ga_{28.9}$ alloy sample contains two phases. These are mainly body-centered tetragonal (tetragonally distorted L2$_1$) phase with the lattice parameters of $a = b = 0.5345$ nm, $c = 0.716$ nm and some amount of L2$_1$ phase with $a = b = c = 0.5885$ nm (see Fig. 5). Even though superstructure reflections for L2$_1$ phase at this pattern are hard to be seen it is unlikely that cooling down to $T =$ 78 K causes significant atomic disorder in this phase of alloy.

Conclusions on the sample structures based on the results of XRD measurements are supported also by RT optical image of the sample surface - martensitic variants dominate on the surface of the sample previously cooled down the liquid nitrogen temperature (see Fig. 6).

The obtained lattice parameters for cubic austenite and martensitic tetragonal phases nicely agree with the results obtained in the literature. Zhu *et al.* the marentsitic phase for $Fe_{50}Mn_{22.5}Ga_{27.5}$ HA at $T = 90$ K have been indexed as a body-centered tetragonal structure with the lattice parameters $a = b$ $= 0.5328$ nm and $c = 0.7113$ nm and largest lattice distortion, $(c - a)/a = 33.5\%$ among all the reported FSMAs [5]. The similar result has been obtained by Omori *et al.* for
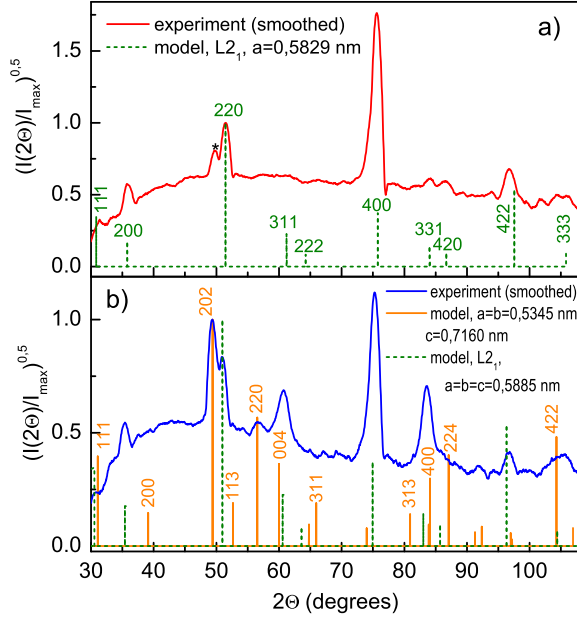
5

Figure 5: Smoothed RT experimental XRD patterns for bulk $Fe_{45.2}Mn_{25.9}Ga_{28.9}$ alloy sample after: a) its heating up to $T = 373$ K (red line) and b) after cooling down to $T = 78$ K (blue line) together with calculated stroke-diagrams for stoichiometric Fe_2MnGa alloy with $L2_1$ (green lines) and tetragonal (yellow line) types of lattice.

Figure 6: RT optical image of the $Fe_{45.2}Mn_{25.9}Ga_{28.9}$ alloy sample surface subjected to heating up to $T=373$ K (upper panel) and cooling down to $T=78$ K (bottom panel).

$Fe_{44}Mn_{28}Ga_{28}$ HA - martensitic phase has been identified as non-modulated tetragonal one with the lattice parameters of $a = b = 0.5368$ nm, $c = 0.7081$ nm and the $c/a = 1.319$, where the distorted $L2_1$ structure is taken as the unit cell of the non-modulated tetragonal martensite. The volume change due to the forward transformation $\Delta V/V$ is +0.73 % [6].

In our case lattice distortion $(c - a)/a$ of the tetragonal phase is 34.5 %. Forward MT induces the volume increase of $\Delta V/V = 3.28$ %.
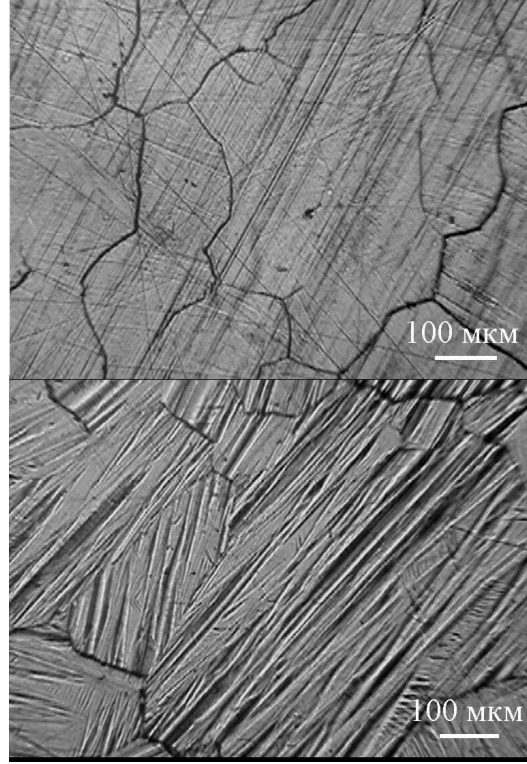
Abnormally intense (400) reflection for $L2_1$ phase indicates on the presence of some texture in polycrystalline $Fe_{45.2}Mn_{25.9}Ga_{28.9}$ alloy sample.

3.3. Magnetic properties

Magnetic properties of bulk $Fe_{45.2}Mn_{25.9}Ga_{28.9}$ polycrystalline alloy sample are presented on Figs. 7 and 8. The temperature dependence of magnetization $M(T)$ obtained at weak ($H = 500$ Oe)

magnetic field exhibits two definite drops upon sample heating from $T = 4$ K. Reverse sample cooling from $T = 350$ K causes an increase of magnetic moment also at two steps started at $T \approx 248$ and 153 K. It is clearly seen that the low-temperature peculiarity does not depend on heat-treatment direction while the high temperature one does (see Figs. 7 and 8). Such a behavior of $M(T)$ and dM/dT dependencies supports two-phase nature of the sample revealed by XRD data: low-temperature peculiarity at $T \approx 150$ K can be definitely ascribe to the Curie temperature of the cubic $L2_1$ phase while high-temperature one is concerned with MT between tetragonal and cubic phases.

It can be concluded that the Curie temperature for tetragonally distorted $L2_1$ phase at least, not less than $T \approx 315$ K. Thus, for $150 \leq T \leq 329$ K temperature range we have the deal with nonmagnetic (i. e. PM) $L2_1$ phase and FM tetragonal matrensitic one.

Increase in the external magnetic field up to 50 kOe drastically changes the $M(T)$ and dM/dT dependencies for $Fe_{45.2}Mn_{25.9}Ga_{28.9}$ alloy: low-temperature peculiarities concerned with the Curie temperature of $L2_1$ phase disappear, A_f temperature increases up to about 329 K, the hysteresis between $M(T)$ plots obtained on the sample heating and cooling and determined as A_f - M_s converges from $\Delta T_{H=500Oe} \approx 70$ K down to $\Delta T_{H=5kOe} \approx 63$ K (see Figs. 7 and 8). It should be noted here that the saturation magnetization of $Fe_{45.2}Mn_{25.9}Ga_{28.9}$ alloy at $T = 4$ K and $\mu_0 H = 5$ T $M_{sat} = 79$ emu/g (or 3.26 μ_B/f.u.) is close to those reported in the literature: 71 emu/g for $Fe_{44}Mn_{28}Ga_{28}$
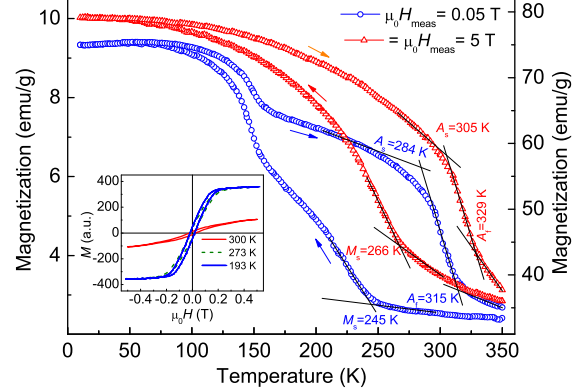

Figure 7: Temperature dependencies of the magnetization of $Fe_{45.2}Mn_{25.9}Ga_{28.9}$ polycrystalline alloy measured in a weak ($H = 500$ Oe, left scale) and strong ($H=50000$ Oe, right scale) magnetic fields on sample heating and cooling. Inset shows magnetization hysteresis loops of alloy taken at different temperatures upon sample cooling.

alloy, 83 emu/g for $Fe_{43}Mn_{28}Ga_{29}$ alloy, 93.8 emu/g for $Fe_{50.0}Mn_{22.5}Ga_{27.5}$ alloy [5, 6, 7]. Recall that calculated magnetic moments for $L2_1$ and $L1_0$ phases are $\mu = 2.01$ and 6.35 $\mu_B/f.u.$, respectively. Therefore, taking into account two-phase nature of $Fe_{45.2}Mn_{25.9}Ga_{28.9}$ alloy, experimentally determined its saturation magnetization value looks reasonable.

According to the results of first-principle calculations the specific magnetic moments of the $L2_1$ and tetragonal phases differ more than three times. Concerning $M(T)$ dependence obtained at $H = 500$ Oe field (see Fig. 7) the amount of $L2_1$ phase in $Fe_{45.2}Mn_{25.9}Ga_{28.9}$ alloy at $T \approx 150$ K is comparable with tetragonal one. Therefore, almost invisibleness of FM to PM transition
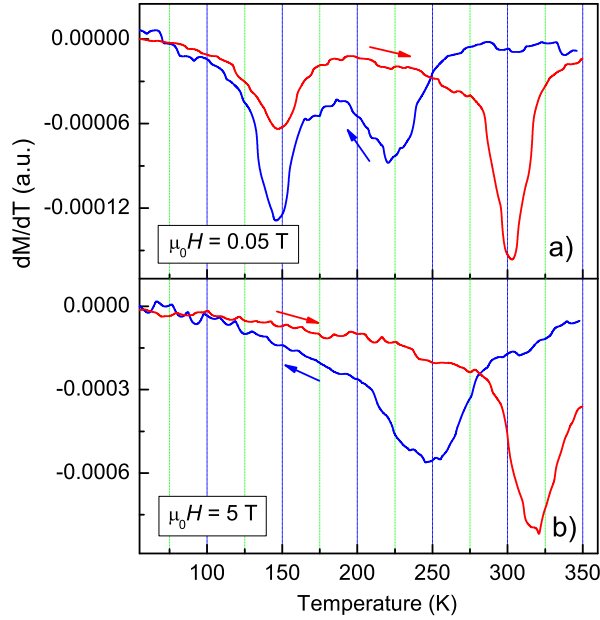
Figure 8: Temperature derivatives of $M(T)$ plots for $Fe_{45.2}Mn_{25.9}Ga_{28.9}$ HA obtained at different measuring fields on sample heating and cooling.

related to $L2_1$ phase in the $M_{H=50kOe}(T)$ plot can be explained by complete $L2_1$ to tetragonal phase transition induced by strong magnetic field rather than smearing in temperature of FM to PM transition in $L2_1$ phase.

The high-temperature shift of the MT temperatures with magnetic field H once again supports an assumption that the Curie temperature for a tetragonal phase is not less than $T \approx 329$ K.

It is known that the magnetic field is the factor which can play an important role in thermodynamical processes. For example, the effect of a magnetic field on the temperatures of direct and reverse marten-

sitic transformations was investigated for $Ni_{2+x}Mn_{1-x}Ga$ alloys in a pioneering paper of Dikstein *et al.* [18]. The shift of the phase equilibrium temperature under the influence of magnetic field can be expressed by Krivoglaz-Sadovsky equation [19]:

$$\Delta T = T_0(m_1 V_1 - m_2 V_2)\Delta H/q, \qquad (1)$$

where T_0 is the temperature of phase transition without magnetic field, $m_{1,2}$ and $V_{1,2}$ are magnetic moments and volumes of initial (1) and final (2) phases, ΔH is the change of external magnetic field, q is the specific heat of transition. For the case of reverse MT in $Fe_{45.2}Mn_{25.9}Ga_{28.9}$ alloy transition from FM martensitic phase to PM austenite $L2_1$ phase ($m_2 = m_{L21} \approx 0$ for $150 \leq T \leq 312$ K temperature range) this equation can be written as:

$$\Delta T = T_0 m_1 V_1 \Delta H/q, \qquad (2)$$

It is clear that for our case external magnetic field should induce a positive shift of phase transition temperature. Indeed, according to the results shown in Figs. 7 and 8 this shift can be evaluated as $\Delta T = A_f(H = 50kOe)$ - $A_f(H = 500Oe) \approx 14$ K for reverse MT or $\Delta T = M_s(H = 50kOe)$ - $M_s(H = 500Oe) \approx 21$ K for direct MT.

Magnetization hysteresis loops for $Fe_{45.2}Mn_{25.9}Ga_{28.9}$ polycrystalline alloy sample indicate on its rather high coercivity $H_c \approx 200$ Oe and magnetization saturation field $H_s \approx 2000$ Oe (see inset in Fig. 7).

3.4. Transport properties

Figure 9 shows the temperature dependencies of resistance $R(T)$ and DC magnetic sus-

ceptibility $\chi(T)$ for bulk $Fe_{45.2}Mn_{25.9}Ga_{28.9}$ alloy obtained at very weak measuring magnetic field. Increase in temperature from $T = 78$ K causes a nearly linear growth of resistance with the positive temperature coefficient of resistivity (TCR). At $T \approx 175$ K small break of the $R(T)$ plot can be seen, TCR value becomes a little bit smaller. At $T \approx 272$ K resistance rapidly growths by about 13 % indicating start of reverse MT in an alloy. At $T \approx 299$ K reverse MT is finished and resistance of alloy starts to decrease almost linearly with temperature. It should be noted here that the temperatures of the peculiarities on the $\chi(T)$ plot coincide with those on the $R(T)$ plot obtained on the sample heating. Taking into account the results of magnetic measurements (see Figs. 7 and 8) low-temperature break of the TCR value can be definitely ascribe to the FM to PM transition in $L2_1$ phase of an alloy. Indeed, electron-magnon (spin-disorder) scattering usually reaches its maximum near the Curie temperature; above T_C the spin-disorder mechanism is independent of T. Therefore, for some ferromagnetic metals and alloys (including FM HA), a distinct change in the slope of the $\rho(T)$ dependence can be expected at T_C [20, 21, 22, 23].

Upon sample cooling from $T = 425$ K resistance follows the same as on the heating way up to $T \approx 299$ K where some break of the negative TCR value can be seen. The rapid drop of resistance at $T \approx 195$ K indicates on the start of the forward MT which is finished at $T \approx 169$ K. Thus, MT in $Fe_{45.2}Mn_{25.9}Ga_{28.9}$ alloy causes the significant changes of the resistance value and the change of the TCR
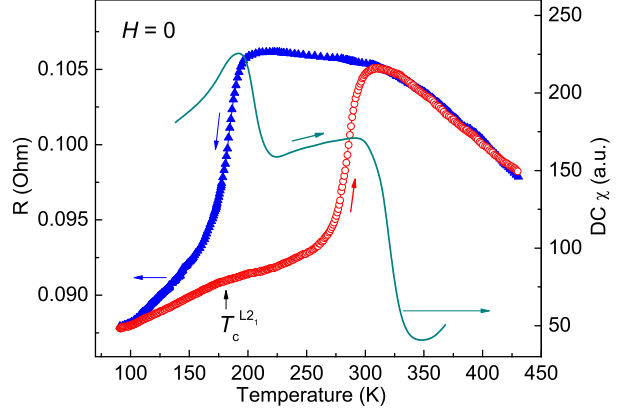

Figure 9: Temperature dependencies of resistance for bulk $Fe_{45.2}Mn_{25.9}Ga_{28.9}$ HA obtained on sample heating and cooling at zero magnetic field (symbols, left scale) and DC magnetic susceptibility obtained at $H_{meas} \approx 5$ Oe upon sample heating (line, right scale).

sign. Such a behavior is the direct consequence of the differences in the electronic structures of these phases, namely DOS values at E_F for $L2_1$ and tetragonal phases of Fe_2MnGa alloy (see Fig. 1).

It should be mentioned here that the calculated value of resistivity of $Fe_{45.2}Mn_{25.9}Ga_{28.9}$ alloy sample shows unreasonably high-value $\rho_{78K} =3.08$ mΩcm probably due to internal cracks induced by sample cutting and concerned with sample brittleness. Therefore, the values of the resistivity Fe_2MnGa alloys should be treated with caution.

Temperature dependencies of resistivity for bulk $Fe_{45.2}Mn_{25.9}Ga_{28.9}$ HA obtained on sample heating and cooling exhibit huge temperature hysteresis - $\Delta T_R \approx 100$ K. This value is rather close to hysteresis of magnetization

obtained at $H = 500$ Oe - $\Delta T_M \approx 90$ K. Such a huge value of thermal hysteresis of structure and physical properties is probably concerned with great friction between the boundaries of martensite and austenite phases due to large lattice distortion at MT.

3.5. Optical properties

Figure 10 presents calculated interband optical conductivity spectra for perfectly ordered stoichiometric Fe_2MnGa alloy with $L2_1$ and $L1_0$ types of atomic order. Both spectra are characterized by the set of interband transitions which form interband absorption peak at $0 \leq \hbar\omega \leq 5$ eV energy range. However, this peak for $L2_1$ phase has a larger intensity and is manifested more definitely. This result looks as unexpected considering noticeable difference in energy dependencies of the DOS values for these phases (see Fig. 1).
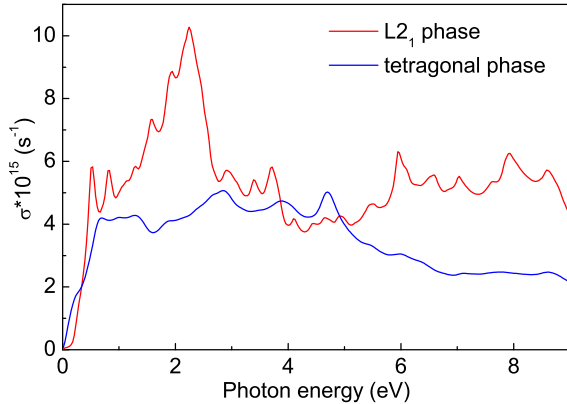

Figure 10: Calculated interband optical conductivity spectra of stoichiometric Fe_2MnGa alloy in cubic $L2_1$ and tetragonal phases.

Experimental optical conductivity spectra of bulk $Fe_{45.2}Mn_{25.9}Ga_{28.9}$ HA at different temperatures (i. e. in different structural states) are shown on Fig. 11. In order to obtain confidently the austenitic and martensitic states in the alloy, the optical measurements were carried out at $T = 373$ K and $T = 173$ K on the sample preliminary heated and cooled up to 573 and down to 78 K, respectively. Such an approach allows us definitely to fix martensitic and austenite phases in alloy and to minimize the temperature effect on the optical properties of the alloy. Unlike theoretical predictions the optical conductivity spectra for austenitic and martensitic phases look rather similar and both are characterized by broad intense interband absorption band located at $\hbar\omega \approx 1.2$ eV.

To the best of our knowledge, there are few publications devoted to the experimental study of the optical properties of Fe_2MnGa alloys [24, 25]. Thus, Král investigated the optical properties of several electrolytically polished bulk Fe-Mn-Ga alloys near the stoichiometry 2:1:1. All the investigated by him alloys of different compositions (and probably different crystalline structures) demonstrate rather similar optical properties [25]. Furthermore, the optical conductivity spectrum for bulk $Fe_{46.6}Mn_{24.2}Ga_{29.2}$ HA obtained by Král in the spectral shape and absolute value practically coincides with that for $Fe_{45.2}Mn_{25.9}Ga_{28.9}$ HA studied in a present work and shown on Fig. 11.

Such a similarity of the experimental optical properties of bulk $Fe_{45.2}Mn_{25.9}Ga_{28.9}$ HA in the martensitic and austenitic phases probably can be concerned party with two-phase nature this alloy sample, whose opti-
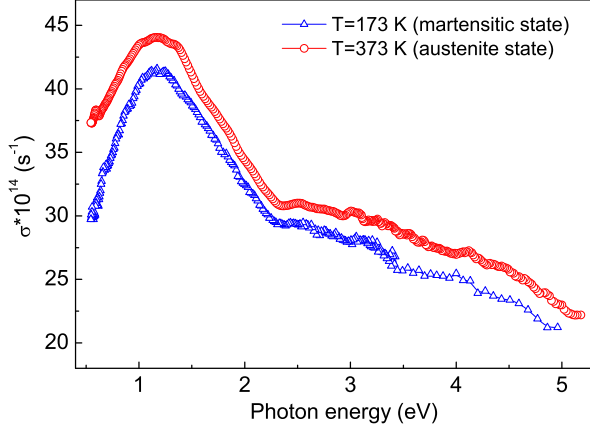
Figure 11: Experimental optical conductivity spectra of bulk $Fe_{45.2}Mn_{25.9}Ga_{28.9}$ HA in austenite (T_{meas} = 373 K, circles) and martensitic (T_{meas} = 173 K, triangles) states.

cal properties predicted to be rather similar. At the same time the two-phase nature of $Fe_{45.2}Mn_{25.9}Ga_{28.9}$ alloy sample was not sufficient for a complete masking of the changes in its magnetic and transport properties induced by MT because of the properties of pure austenitic and martensitic phases differ drastically.

4. Summary

1. First-principle calculations revealed that the stoichiometric Fe_2MnGa alloy with $L2_1$ and $L1_0$ types of the atomic order has noticeable different $N(E)$ dependencies (especially at E_F), exhibits three times different magnetic moments of the formula units and manifests qualitatively similar calculated interband optical conductivity spectra.

2. Temperature-induced direct martensitic transformation in $Fe_{45.2}Mn_{25.9}Ga_{28.9}$ Heusler alloy causes a rapid decrease in its resistivity value, changes of the TCR sign from negative to positive and leads to the transition from PM to FM state.

3. Direct and reverse MT in $Fe_{45.2}Mn_{25.9}Ga_{28.9}$ Heusler alloy demonstrate about $\Delta T \approx$ 90 - 100 K hysteresis in critical temperatures manifested by temperature dependencies of resistance and magnetization.

4. External magnetic field of $H = 50$ kOe causes the positive shift of the critical temperatures and reduces temperature hysteresis width.

5. Experimentally observed changes in the magnetic and transport properties of $Fe_{45.2}Mn_{25.9}Ga_{28.9}$ alloy induced by MT nicely can be explained by the changes in the electronic structures of alloy upon transition from the austenitic to martensitic phase.

6. MT does not lead to visible changes in the experimental OC spectra of $Fe_{45.2}Mn_{25.9}Ga_{28.9}$ alloy because of partly its two-phase nature and not very significant difference in calculated optical properties of these phases.

5. Acknowledgments

References

[1] C. A. Jenkins, A. Scholl, R. Kainuma, H. J. Elmers, and T. Omori, Appl. Phys. Lett. **100**, 032401 (2012).

[2] K. Ullakko, J. K. Huang, C. Kanter, V. V. Kokorin, and R. C. O'Handley, J. Appl. Phys. **81**, 5416 (1997).

[3] Z. H. Liu, M. Zhang, Y. T. Cui, Y. Q. Zhou, W. H. Wang, and G. H. Wua, X. Zhang, and Gang Xiao, Appl. Phys. Lett. **82**, 424 (2003).

[4] L. I. Manosa, A. Planes, Ch. Somsen, Ch. Fell, and M. Acet, J. Phys. IV France **11**, Pr8-245-Pr8-249 (2001).

[5] W. Zhu, E. K. Liu, L. Feng, X. D. Tang, J. L. Chen, G. H. Wu, H. Y. Liu, F. B. Meng, and H. Z. Luo, Appl. Phys. Lett. **95**, 222512 (2009).

[6] T. Omori, K. Watanabe, X. Xu, R.Y. Umetsu, R. Kainuma and K. Ishida, Scripta Materialia **64**, 669 (2011).

[7] T. Omori, K. Watanabe, R. Y. Umetsu, R. Kainuma, and K. Ishida, Appl. Phys. Lett. **95**, 082508 (2009).

[8] V. V. Khovaylo, T. Omori, K. Endo, X. Xu, R. Kainuma, A. P. Kazakov, V. N. Prudnikov, E. A. Ganshina, A. I. Novikov, Yu. O. Mikhailovsky, D. E. Mettus, and A. B. Granovsky, Phys. Rev. B, **87**, 174410 (2013).

[9] A. N. Vasilev, A. D. Bozhko, V. V. Khovailo, I. E. Dikshtein, V. G. Shavrov, V. D. Buchelnikov, M. Matsumoto, S. Suzuki, T. Takagi, and J. Tani, Phys. Rev. B **59**, 1113 (1999).

[10] P. Entel, V. D. Buchelnikov, V. V. Khovailo, A. T. Zayak, W. A. Adeagbo, M. E. Gruner, H. C. Herper and E. F. Wassermann, J. Phys. D: Appl. Phys. **39**, 865 (2006).

[11] T. Krenke, X. Moya, S. Aksoy, M. Acet, P. Entel, Ll. Mańosa, A. Planes, Y. Elerman, A. Yüceld, E. F. Wassermann, Jour. Magn. Magn. Mater. **310**, 2788 (2007).

[12] Y. V.Kudryavtsev, V. V. Nemoshkalenko Y. P. Lee, K. W. Kim, J. Y. Rhee and J. Dubowik, J. Appl. Phys., **90**, 2903 (2001).

[13] Y. P. Lee, Y. V. Kudryavtsev, V. V. Nemoshkalenko, R. Gontarz, and J. Y. Rhee, Phys. Rev. B **67**, 104424 (2003)

[14] I. I. Sasovskaya, S. A. Shabalovskaya, A. I. Lotkov, Jour. Exp. Theor. Phys., **77**, 2341 (1979). (in Russian).

[15] J. F. Wan and J. N. Wang, Physica B, **355**, 172 (2005).

[16] E. A. Ganshina, A. I. Novikov, G. S. Zykov, D. E. Mettus, A. P. Kazakov, R. Kainuma, V. V. Khovailo, V. N. Prudnikov, and A. B. Granovskij, Phys. Solid State **55**, 1866 (2013).

[17] Y. V. Kudryavtsev, A. E. Perekos, N. V. Uvarov, M. R. Kolchiba, K. Synoradzki,

and J. Dubowik, Jour. Appl. Phys. **119**, 205103 (2016).

[18] I. Dikshtein, V. Koledov, V. Shavrov, A. Tulaikova, A. Cherechukin, V. Buchelnikov, V. Khovailo, M. Matsumoto, T. Takagi and J. Tani, IEEE Transactions on Magnetics, **35**, 3811 (1999).

[19] M. A. Krivoglaz and V. D. Sadovsky, Physics of Metals and Metalography, **18**, 502 (1964) (in Russian).

[20] S. Majumdar, M. K. Chattopadhyay, V. K. Sharma, K. J. S. Sokhey, S. B. Roy, and P. Chaddah, Phys. Rev. B **72**, 012417 (2005).

[21] S. Bose, J. Kudrnovsky, and V. Drchal, World J. Eng. **9**, 13 (2012).

[22] J. Kudrnovsky, V. Drchal, I. Turek, S. Khmelevskyi, J. K. Glasbrenner, and K. D. Belashchenko, EPJ Web Conf. **40**, 12001 (2013).

[23] J. Barth, G. H. Fecher, B. Balke, S. Ouardi, T. Graf, C. Felser, A. Shkabko, A. Weidenkaff, P. Klaer, H. J. Elmers, H. Yoshikawa, S. Ueda, and K. Kobayashi, Phys. Rev. B **81**, 064404 (2010).

[24] Y. V. Kudryavtsev, N. V. Uvarov, V. N. Iermolenko, I. N. Glavatskyy, J. Dubowik, Acta Mater. **60**, 4780 (2012).

[25] D. Král, *Optical and magneto-optical properties of Heusler compounds*, Master thesis, Institute of Physics of Charles University, Prague 2017.